Phase Transformations and Tensile Properties of Ti-10V-2Fe-3Al

T. W. DUERIG, G. T. TERLINDE, AND J. C. WILLIAMS

The effect of heat treatment on the microstructure of the metastable β-Ti alloy Ti-10V-2Fe-3Al has been studied using light and electron metallography, analytical electron microscopy, and X-ray diffraction. A survey of the effects of microstructure on tensile properties of the alloy also has been conducted. It has been found that the alloy contains inclusions which are rich in Ti, S, Si, and P. The alloy has been shown to form ω-phase both athermally and isothermally. The isothermal ω can have either an ellipsoidal or a cuboidal morphology. The reasons for this are enumerated. The formation of α-phase has been studied, and three distinct modes of formation are described. A stress induced orthorhombic martensite also has been observed. The effect of this stress induced product on tensile behavior is discussed. The relative roles of inclusions and α-phase precipitates in the tensile fracture also have been examined.

DEMANDS for high strength light-weight alloys have been steadily increasing in recent years. Although the well established α and $\alpha + \beta$ titanium alloys (such as Ti-6Al-4V) have successfully met many of these demands, they are unsuited for thick section applications due to their extremely rapid decomposition kinetics. This has shifted research interests to the β-Ti alloys, so called because the high temperature bcc phase (β) is chemically stabilized and can be retained upon quenching. When compared to the α and $\alpha + \beta$ alloys, β alloys enjoy the advantages of increased strength-to-density ratios, (some 20 pct higher than Ti-6Al-4V, for example), improved formabilities, lower thermal processing costs, and most importantly, improved deep hardenabilities.

Ti-10V-2Fe-3Al is a relatively new β-Ti alloy, in which the high temperature β-phase is stablized by nominal alloying additions of 2 wt pct Fe and 10 wt pct V. The 3 pct Al is a natural ingredient in the master alloy and acts as a solid solution strengthener for the low temperature precipitating α-phase (HCP). This particular alloying combination results in a nominal β-transus of ~800 °C, which is relatively high when compared to other β alloy systems. Generally the more heavily β-stabilized alloys (such as β-III, Ti-8V-8Mo-2Fe-3Al, and so forth) suffer from higher densities, higher manufacturing costs, and slower age hardening kinetics than Ti-10V-2Fe-3Al. This paper describes the results of a research program conducted to identify the various phase transformations of Ti-10-2-3, and to relate these to basic tensile properties.

T. W. DUERIG, formerly at Carnegie-Mellon University, is now at Brown, Boveri & Cie, AG, Baden, Switzerland, G. T. TERLINDE and J. C. WILLIAMS are with the Department of Metallurgical and Materials Science, Carnegie-Mellon University, Pittsburgh, PA 15213.

Manuscript submitted August 2, 1979.

EXPERIMENTAL

The material used in this study originated from Timet heat No. P-1452. The specific heat chemistry is:

Element	V	Fe	Al	O	N	C	Si	Ti
Concentration, (wt pct)	10.3	2.2	3.2	0.15	0.009	0.016	0.04	Balance

The β-transus was measured as 805 ± 3 °C, somewhat high compared to other 10-2-3 heats. This probably reflects the oxygen content which is on the high side of the normal range. The thermomechanical processing began with a 3200 kg pound ingot which was upset forged 35 pct at 1120 °C, drawn to an 40 cm^2, and subsequently forged to a plate of 18 cm × 4.5 cm cross-section. The slab was then cut and hot rolled from 730 °C to a 2.5 cm × 11.5 cm plate.

All subsequent heat treatments were done in laboratory-type apparatus using small specimens. Treatments above 600 °C were done by vacuum encapsulating specimens wrapped with Ta foil. Below 600 °C, treatments were performed in a liquid nitrate salt bath.

Metallographic specimens were electropolished in a 5 pct H_2SO_4 + 1 pct HF + balance methanol solution at a closed circuit voltage of 21 V. The primary etchant was prepared with equal parts of 10 pct oxalic acid and 1 pct HF in water.

Thin foils for Transmission Electron Microscopy (TEM) were prepared in a Fishione twin jet electropolishing unit with either a 6 pct percloric + 31 pct butanol + 63 pct methanol solution, or a 5 pct H_2SO_4 + 95 pct methanol solution chilled to —50 °C. The foils were examined in a variety of electron microscopes. Instruments used were a JEOL 100B, JEOL 100C, and JEOL 100CX TEMSCAN equipped with a Kevex Quantex energy dispersive X-ray spectrometer. Scanning Electron Microscopy (SEM) was done on a JSM-35.

Tensile testing was performed on an Instron machine using a clip-on extensometer. The strain rate

ISSN 0360-2133/80/1211-1987$00.75/0

was 0.00055 s^{-1}, and the tensile specimen gage sections were 0.640 cm in diam and 3.2 cm in length. Specimens were pulled with the rolling direction parallel to the tensile axis.

RESULTS AND DISCUSSION

I. Microstructural

For organizational purposes, the results of the microstructural study of 10-2-3 can be sub-divided into sub-sections. These are listed below along with the content of each sub-section:

A) *Thermomechanically Processed and/or Annealed Microstructures*. Characterization of the hot rolled material and discussion of the various microstructural changes which occur during solution treating.

B) *Quenching Transformations*. Discussion of the athermal β to ω transformation.

C) *Isothermal Aging Transformations*. Description of the isothermal β-ω reaction and three morphologies of α precipitation.

D) *Stress Assisted Transformations*. Discussion of the martensitic transformation of β to α'' orthorhombic martensite during straining.

Each of these topics will be separately discussed. The effect of these various microstructural modifications on the tensile properties of 10-2-3 will be discussed in a separate section.

A) THERMOMECHANICALLY PROCESSED AND ANNEALED STRUCTURES

Other work[1-3] has shown that minor modifications in thermomechanical processing (TMP) histories influence 10-2-3 microstructures quite strongly. For example:

1) High deformation rates and high temperatures encourage dynamic recrystallization, leading to a somewhat equiaxed β-grain structure. Low temperatures and deformation rates, on the other hand, result in a highly deformed β-grain structure.

2) Volume fraction of primary α (defined as α present at the temperature of TMP completion) can be directly related to TMP temperature. High volume fractions of α_p also tend to retard recrystallization rates during TMP.

3) High deformation rates tend to break-up primary α (α_p) particles, and thereby reduce their aspect ratio. High deformation rates also tend to increase the propensity for recrystallization both during and after TMP.

Results from only one TMP schedule will be discussed in this paper. Thus, it is appropriate to carefully document the as-rolled microstructure since it represents the starting point for all subsequent microstructural modifications.

Figure 1(*a*) shows the microstructures of 10-2-3 as hot rolled by Timet in the aforementioned manner. Optical examination of large areas of the polished and etched surface of the hot rolled plate showed that there are discrete bands present, which contain a lower α_p volume fraction than the surroundings. By heating to just below the β-transus and quenching, (Fig. 1(*b*), the discrete nature of the bands becomes more obvious. Scanning Transmission Electron Microscopy (STEM) X-ray techniques were successful in demonstrating the bands to be enriched in Fe by as much as 50 pct of the nominal Fe content while having the nominal composition with respect to all other elements. Clearly, decomposition reactions occurring within these discrete bands will differ from reactions occurring in the surrounding "normal" material. Since the total volume fraction of compositionally "irregular" or banded material is very low, we will discuss only reactions occurring in the compositionally "normal" material. To assure ourselves that our conclusions were based on only these "normal" regions, all small area investigations (such as TEM), were either accompanied by low magnification optical examinations, or in cases where this was impossible, were repeated several times in different macroscopic

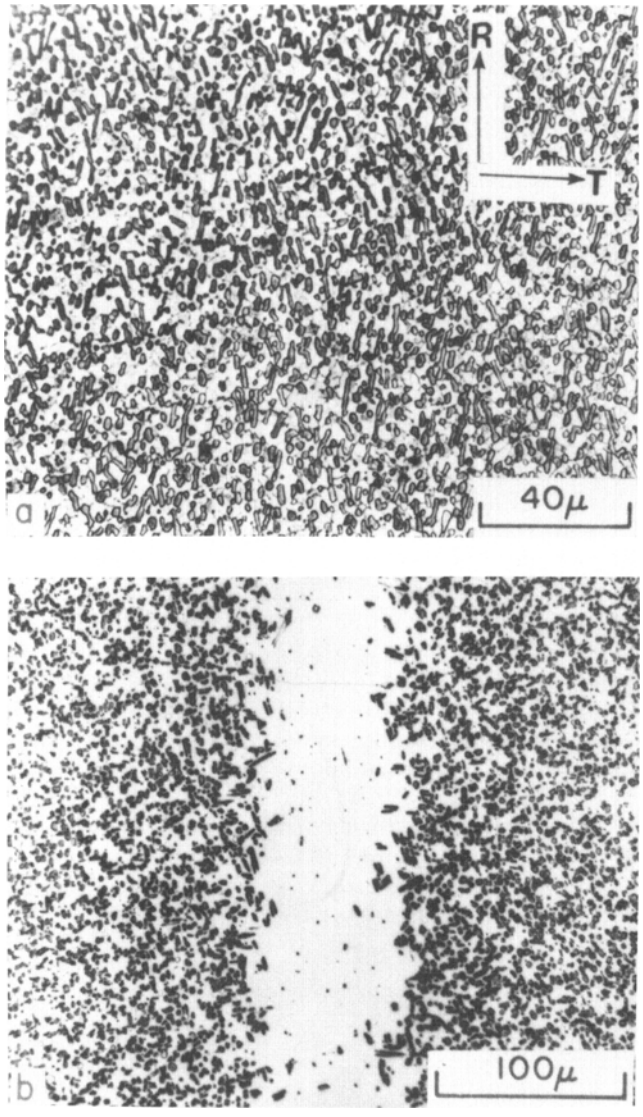

Fig. 1—Optical micrographs of Ti-10V-2Fe-3Al (*a*) as hot rolled and prior to aging, and (*b*) as solution treated in the $\alpha + \beta$ field (800 °C + furnace cooled) to emphasize chemical banding. The rolling direction (R) and the short transverse direction (T) are shown. Part (*b*) is oriented the same way.

sample areas. Thus, a statistically reliable result was assured.

TEM investigations of the as-rolled structure show that both the β matrix and the α_p are polygonized. More detailed examination revealed a small amount of fine α on subgrains, and a uniform dispersion of athermal ω, which will be discussed below.

Solution treating subsequent to TMP can be performed either above the 805 °C β-transus (β-ST) or below it ($\alpha + \beta$-ST). Examples of both are given in Fig. 2. From these it can be seen that no athermal martensite forms while quenching 10-2-3 from above the β-transus. Thus the M_s of the alloy must lie beneath room temperature. Inclusions of a 1 μm average diam are more readily observed in Fig. 2(*a*), but are present in all conditions. Fig. 3(*a*) shows one of the larger inclusions in TEM bright field. Since these inclusions were typically 1 μm or smaller in diameter, analysis by electron microprobe or SEM/EDX was not feasible. Analysis by STEM/EDX was relatively easy, however, and typical X-ray spectra of both the matrix and the inclusion are shown in Fig. 3(*b*). Repeated analysis of these inclusions has shown that the inclusion compositions are somewhat variable but typically fall in the following atomic percent ranges:

Silicon	2.0 to 4.0
Phosphorus	13.0 to 15.0
Sulfur	3.0 to 6.5
Titanium	75. to 80.

Such inclusions (as well as the aforementioned banding) are common not only to 10-2-3, but to most β-Ti alloys, making the results of this paper pertinent to most commercial heats of β-Ti alloys.

Of the various microstructural modifications brought about by solution treating the as-rolled material, the most rapid is the equilibration of α-phase volume fraction. Figure 4 relates equilibrium α to solution treatment (ST) temperature. This data was obtained by a Quantimet 7000, and independently

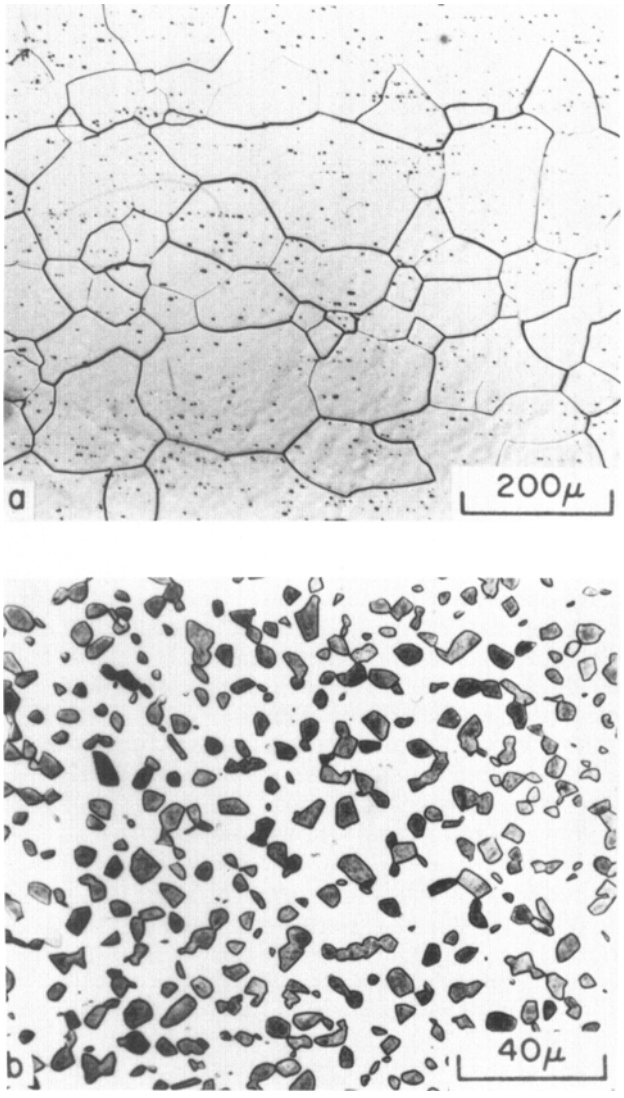

Fig. 2—Optical micrographs of solution treated Ti-10-2-3: (*a*) β-ST (850 °C—15 m) and water quenched, and (*b*) $\alpha + \beta$-ST (730 °C—10,000 m) and water quenched.

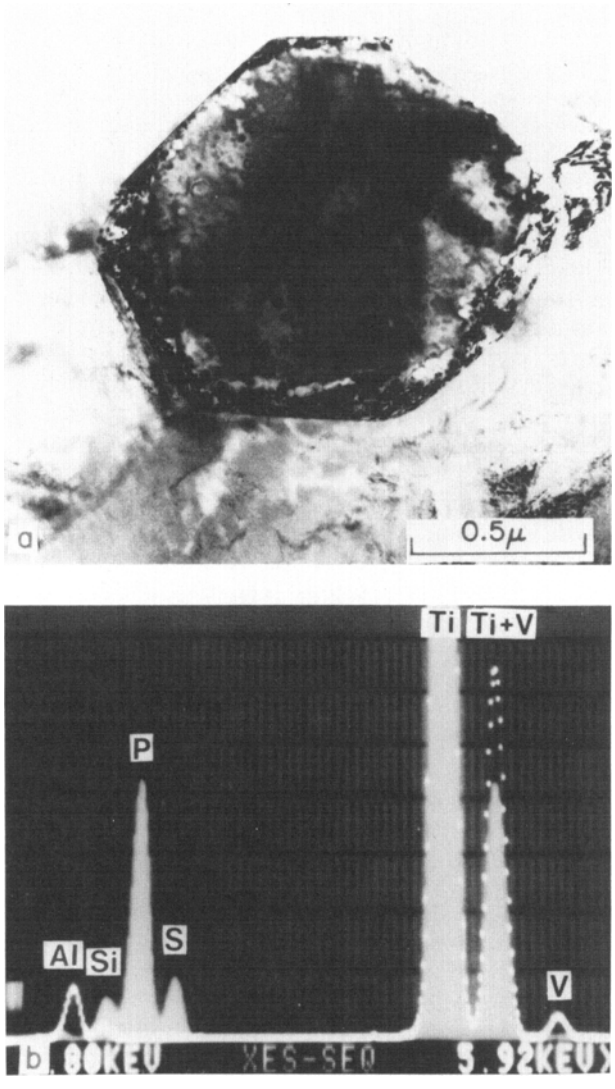

Fig. 3—(*a*) Conventional TEM micrograph showing an inclusion in 10-2-3, and (*b*) the energy dispersive X-ray spectra from the inclusion and the adjacent matrix. Matrix spectrum is shown in outline, inclusion spectrum in solid.

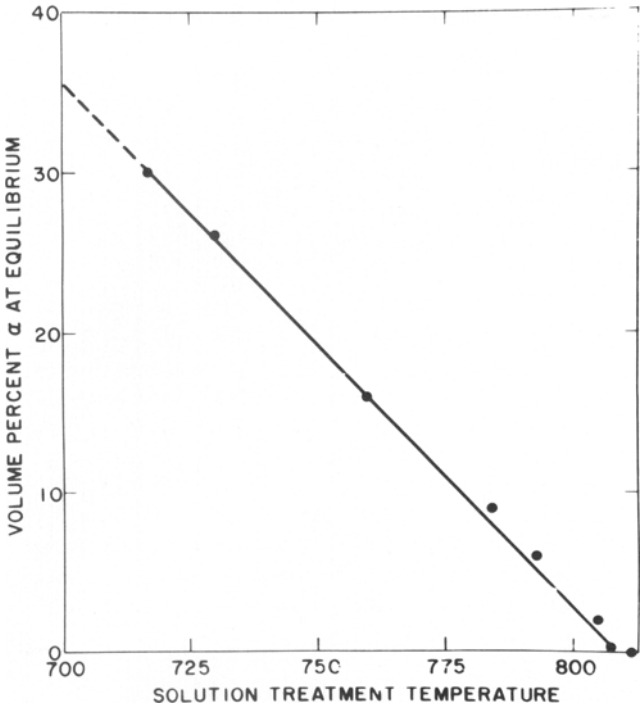

Fig. 4—Plot illustrating the dependence of equilibrium α content on ST temperature.

confirmed by manual quantitative metallography. Equilibration is very rapid due to the high diffusivities of both Fe and V. Five minutes at 850 °C is sufficient to dissolve all α_p in the hot rolled material. Matrix recrystallization has been observed to be extremely rapid during β-ST treatments, but extremely slow when α_p is present due to the pinning effects of the α_p particles. For example, 5 min at 850 °C completely recrystallizes the β grain structure, but 10^4 min at 760 °C has very little effect upon the rolled structure. Grain growth following recrystallization was found to be extremely sluggish. In the presence of α_p, grain growth was found to be slowed by the pinning effect of α_p. During β-ST, growth was found to be slowed by the presence of inclusions. The most important effect of any solution treatment, however, is to control the β-phase stability after subsequent quenching. Clearly, a lower ST temperature will result in a more stable, solute-rich, as-quenched β matrix, and a lower driving force for subsequent decomposition behavior. The importance of this will be shown in the mechanical property discussion.

B) TRANSFORMATION PRODUCTS OF QUENCHING

There are two types of athermal transformation products found in Ti alloys: athermal ω (ω_a) and various martensites. Although both can be found in quenched 10-2-3 specimens, the latter is attributable to quenching strains, rather than to the quench itself, and therefore is more appropriately discussed in a later section where stress assisted transformations are discussed.

The athermal β to ω transformation was shown to

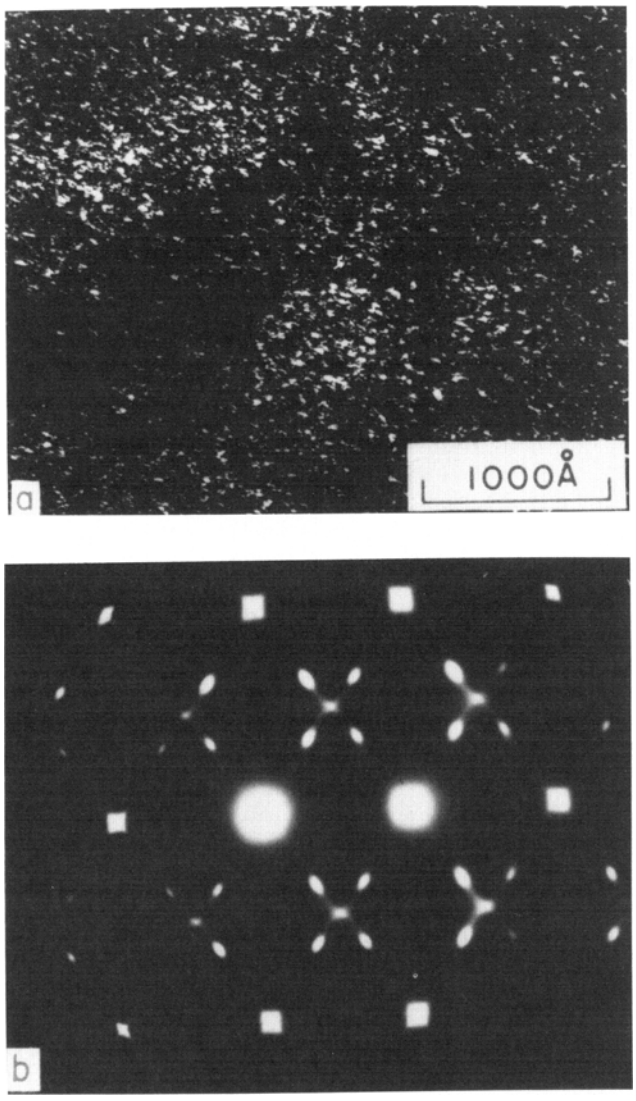

Fig. 5—Athermal ω (ω_{ath}) shown in the β-ST condition: (*a*) TEM dark field, and (*b*) [110] β-zone electron diffraction pattern.

occur uniformly throughout the β-phase in all solution treated and quenched material with less than ~30 vol pct by volume α_p (Fig. 5). Since an understanding of the $\beta \rightarrow \omega_{ath}$ transformation mechanism is crucial to later discussions in this paper, it is necessary that recent work in this area be summarized.

Although verified to be a diffusionless process by rapid quenching experiments,[4] the athermal $\beta \rightarrow \omega$ transformation is not martensitic in the classical sense. De Fontaine and others[5,6] have shown that the instability of the β-matrix with respect to 2/3 <111> longitudinal displacement waves could lead to a local ordering of displaced (111) planes, with a resulting structural transformation. The structure formed by such an event is the ω-phase, which has a hexagonal cell (P6/mmm) with $c/a = 0.613$ and atoms positioned at (0,0,0), (1/3, 2/3, 1/2), and (2/3, 1/3, 1/2). Further, the orientation relation first suggested by Silcock,[7] and which has been shown in many alloys[8,9] is in keeping with the transformation mechanism just discussed. This relation is:

$(0\bar{0}01)_\omega \parallel (1\bar{1}1)_\beta$
$(11\bar{2}0)_\omega \parallel (1\bar{1}0)_\beta$

Energetically, this diffusionless transformation can be understood using the schematic free energy curves of Fig. 6. Shown are the equilibrium α and β curves, as well as the metastable ω curve, for the composition range central to this discussion.

With sufficiently high diffusion rates, ω would form at composition A and the matrix composition would change to C. Thus, the most energetically favorable metastable configuration can be achieved without the intervention of α. During and following a quench, diffusion is not rapid enough to allow this. Between compositions A and B, however, the $\beta \rightarrow \omega$ transformation is energetically favorable without diffusion and can occur if nucleation is sufficiently easy. De Fontaine's displacement wave formation process requires no nucleation *per se* and has little or no activation barrier. Thus, the ω_a is formed immediately upon quenching. At first glance, it may appear that the transformation should go to completion once it has begun but this need not be true. A mechanism has been proposed by Cook,[6] in which the amplitude of the displacement wave discussed above is modulated. This would lead to discrete, regularly spaced wave "packets" from which discrete ω particles are formed. Once the particles are fully developed, the lattice can no longer sustain these elastic waves, and the mechanism for ω formation is lost locally.

C) ISOTHERMAL AGING PRODUCTS

Although the β stability of solution treated and quenched 10-2-3 is somewhat affected by the athermal formation of ω, there remains a considerable driving force available for diffusional transformations. The response of β-ST and quenched 10-2-3 to isothermal aging has been studied and is separately discussed in two categories: i) the isothermal continuation of ω, and ii) the precipitation of α.

i) *Isothermal Omega*. Isothermally aging Ti-10V-

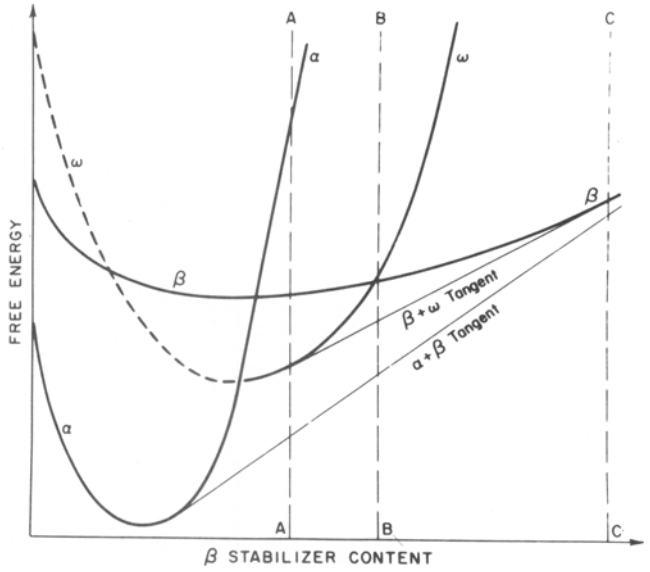

Fig. 6—A schematic representation of the α, β, and ω free energy curves for a hypothetical binary β-stabilized Ti system at an arbitrary temperature.

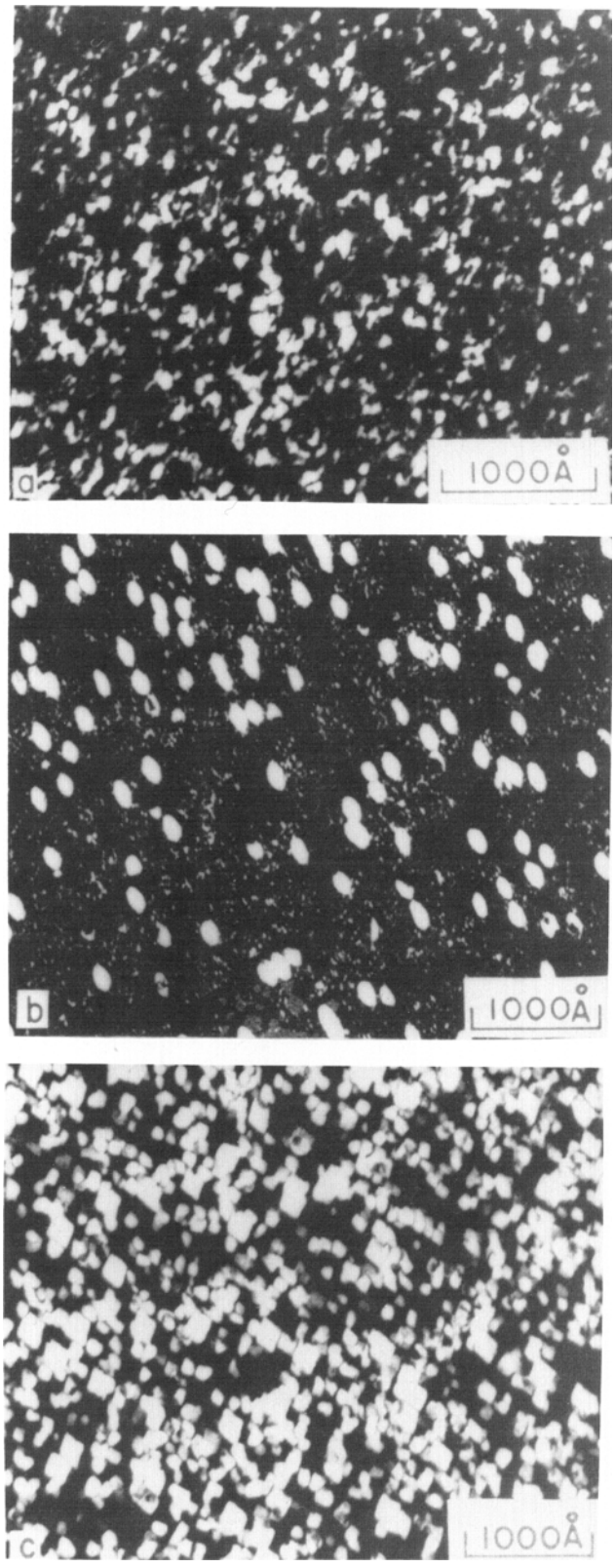

Fig. 7—Dark field TEM micrographs illustrating the three omega morphologies found in β-ST and aged Ti-10-2-3: (*a*) nondescript (250 °C—10,000 m), (*b*) ellipsoidal (400 °C—1 m), and (*c*) cuboidal (400 °C—1 m + 300 C—45 m).

2Fe-2Al at low temperatures (<450 °C) was found to produce a uniform dispersion of isothermal ω (ω_{iso}). Examples of ω_{iso} are shown in Fig. 7. Several unusual observations concerning ω_{iso} were noted. Perhaps the most unexpected of these concerns particle morphology. Earlier studies[8,10,11] have consistently shown that high misfit alloy systems such as Ti-V and Ti-Fe tend to form cuboids of ω, in contrast with the ellipsoids found in low misfit systems. The accepted explanation of this difference is that in high misfit systems, strain energy minimization is important, while in low misfit systems surface energies dominate. Since Ti-10V-2Fe-3Al is a high misfit system, one should expect to find only cuboidal ω. During the early stages of precipitation, however, ellipsoids were found (Fig. 7(*b*)). Continued aging produced a transition to the expected cuboids (Fig. 7(*c*)).

There also were other observations which should be mentioned. First, the growth rates of ω_{iso} are unusually rapid, even at temperatures low enough to be prohibitive to diffusional processes (Fig. 7(*b*) for example). Furthermore, ω_{iso} particles formed at any given temperature are very uniform in size (Fig. 7)*a*) and (*b*)). Duplex aging temperatures result in duplex particle size distributions (Fig. 7(*c*)). Higher aging temperatures consistently result in larger particle sizes and lower particle number densities. Aging times, however, were not found to have an important effect upon particle size. Also of interest is the "hyperfine" particle dispersion of Fig. 7(*b*). This is apparently ω_a which has reformed during the quench after the aging treatment, indicating that the growth of ω_{iso} particles has not significantly stabilized the β-matrix.

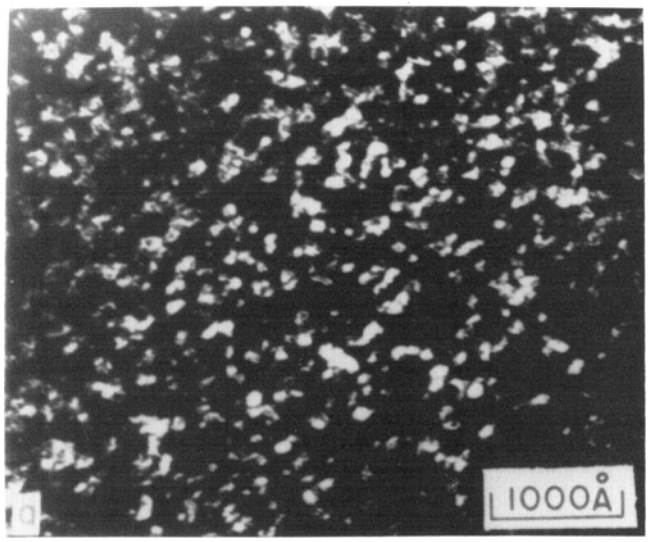

(a)

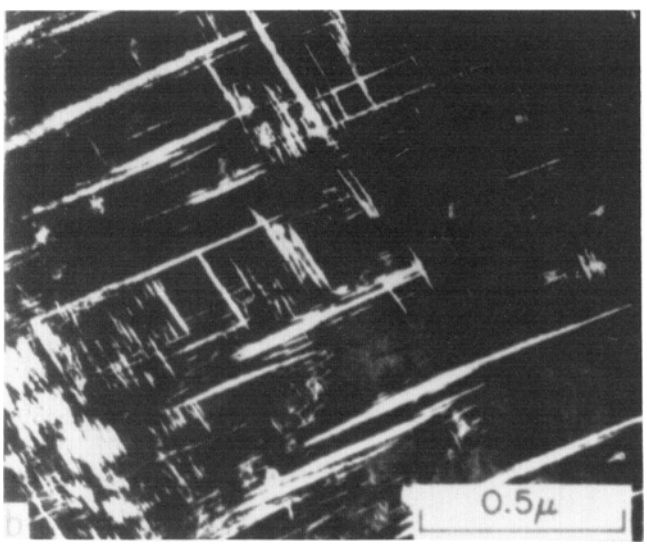

(b)

Fig. 8—Dark field TEM micrographs of the two α morphologies found in Ti-10-2-3- aged at 400 °C for 10 min. (*a*) fine uniform α, which will quickly develop a "stubby" plate morphology, (*b*) sympathetically grown, nonuniform plates with very high aspect ratios.

Many of the above observations are by themselves in conflict with conventional ideas of diffusion controlled nucleation and growth processes. In *toto*, they mandate that a new mechanism of ω_{iso} formation be formulated which more completely explains these unusual observations.

It is appropriate to begin by considering how the $\beta + \omega_a$ matrix changes during rapid heating to an arbitrary aging temperature, T_a. For the ω_a dispersion to become unstable, the relative free energy curves for β and ω must shift in a manner which brings the β-ω curve intersection (composition *B* of Fig. 6) to the left of the alloy composition. Due to the low thermal activation required for ω formation, "quasistatic" embryos of ω_a will persist in a steady state equilibrium even though ω is now unstable to β. Thus the dissolution of ω_a to β occurs over a range of temperatures, with statistically fewer particles present as T_a is increased.

These remnant ω_a particles are subject to random fluctuations in composition. Fluctuations enriching the embryos in Ti will tend to stabilize the ω structure. The important point is that the fluctuations need not be great to stabilize and grow an ω particle if the overall alloy composition is near compsition *B* of Fig. 6. *The particles need only be enriched to composition* B, *not to the tie-line composition denoted in* A *in Fig. 6.* Upon being enriched to composition *B*, particle growth can proceed rapidly by the displacement wave mechanism discussed earlier. Growth should continue until coherency strains become large, and further growth threatens the stability of the particle-matrix interface. After the ω particles are formed, they may then continue to reject solute until the tangent tie-line compositions *A* and *C* are achieved by the ω and the surrounding β respectively.

The observations on ω-phase formation discussed earlier and identified as appearing to be contrary to classical nucleation and growth theory can now be rationalized using a displacement assisted growth mechanism. The dependence of particle size and dispersion density upon aging temperature, and their independence from aging time is an expected result if nucleation upon remnant ω_a particles is assumed. For alloy compositions near composition *B* of Fig. 6, only very small compositional fluctuations are required to stabilize the ω phase. Therefore, the compositions of the β and ω phases are very similar during the early

stages of aging. Thus we should expect ω_a to reform during quenching (the hyperfine particles of Fig. 7(*b*). Further, since the β and ω compositions are similar, their misfit is small, and we should expect ellipsoids. As aging continues, misfit increases, and an ellipsoidal to cuboidal transition is observed.

ii) *Isothermal Alpha.* The equilibrium α-phase in Ti-10-2-3 can form by any one of three nucleation schemes. As will be shown, each nucleation regime results in a distinct morphology and distribution of α. The relative importance of these nucleation modes is controlled by the aging temperature.

At relatively low aging temperatures (below ~450 °C), the appearance of α is preceded by ω. As has been suggested in other β-Ti alloy systems,[8] the ω particles appear to provide preferential nucleation sites for α. Evidence for this is derived from Fig. 8(*a*). Here, extremely fine α of nondescript shape is observed uniformly throughout the β matrix. No preference for nucleation at dislocations or boundaries was observed. The α-phase particle size and distribution closely resembles that of the preceding $\beta + \omega$ structure (Fig. 7(*b*)). Although the precise precipitation mechanism involved is unclear, it has been suggested[10,11] that as ω particles are aged, their associated lattice misfit is increased. Dislocations may then either migrate to, or form at, the $\beta + \omega$ interface. The resulting discontinuity at the β/ω interface may then provide a preferential site for α nucleation. These α nuclei should then rapidly consume the volume occupied by ω-phase, but then only slowly expand into the surrounding matrix. There are two possible reasons for such a biased growth.

1) Since the ω-phase is rich in Ti, the β-ω interface represents a discontinuity in both composition and structure. Although the ω structure may be more conducive to α formation, it is certain that the $\omega \rightarrow \alpha$ transformation requires less diffusion than the $\beta \rightarrow \omega$ transformation.

2) There is evidence that when coherency is lost, the ω particles become unstable. This may also promote α formation.

After the ω-phase is consumed by α, the new α particle may begin to grow into the β matrix. During this later stage, a uniform distribution of small, closely-spaced plates may result.

In Ti alloys, there are two crystallographic types of α: Burger's α, which follows the orientation relationship

$$[111]_\beta \,||\, [11\bar{2}0]_\alpha$$
$$(110)_\beta \,||\, (0001)_a$$

and non-Burger's α; which follows a complex orientation that is yet to be conclusively identified. Although both types of α are common in 10-2-3, α precipitated in this low temperature regime was generally of the first type. Thus, in 10-2-3, Burger's α is observed as a precursor to non-Burger's α. This supports previous work[12] indicating that non-Burger's α is the more stable of the two forms.

Above 400 °C, there is sufficient thermal activation to allow a second nucleation scheme. Here the α-phase nucleates nonuniformly, as high aspect ratio plates bearing no relationship to the previous $\beta + \omega$ dispersion (Fig. 8(*b*)). Although a definite preference for grain boundary nucleation is demonstrated, there is also a definite tendency for the α plates to form in tight clusters within the grains. Since these "patches" are geometrically independent of the aforementioned inhomogeniety bands, we feel this constitutes strong evidence of a "sympathetic" nucleation process. The term "sympathetic nucleation" was first coined by Aaronson[13] to describe the ability of extant α plates to enhance subsequent α nucleation. Although elastic stress fields can often be the cause for this accelerated nucleation, in this case it is more likely that either the dislocation network punched out during formation of previous plates or the α-β surface itself is acting to enhance the nucleation rate.

Although this type of nucleation is active over a wide temperature range, the best support for it is found at 400 °C, where sympathetic plate nucleation must compete with the uniform process discussed above. In this transition regime, plate nucleation is still somewhat slow due to the limited diffusion. Once a plate is nucleated, however, subsequent sympathetic branching is rapid. Thus, a blotchy or patchy α-phase precipitate distribution is observed (Fig. 9). Here the unetched white regions contain the fine uniform precipitation product, while the dark patches are composed of the sympathetic plates. Since the uniform α precipitation process increases β stability uniformly throughout the β matrix, the rate of expansion of the sympathetically nucleated patches slows with increasing aging time and effectively ceases.

A third precipitation regime is evident at higher temperatures (above 650 °C). Here either the sympathetic nucleation process nor the uniform nucleation process appear operative. Instead, a thick α layer forms along grain boundaries with smaller numbers of

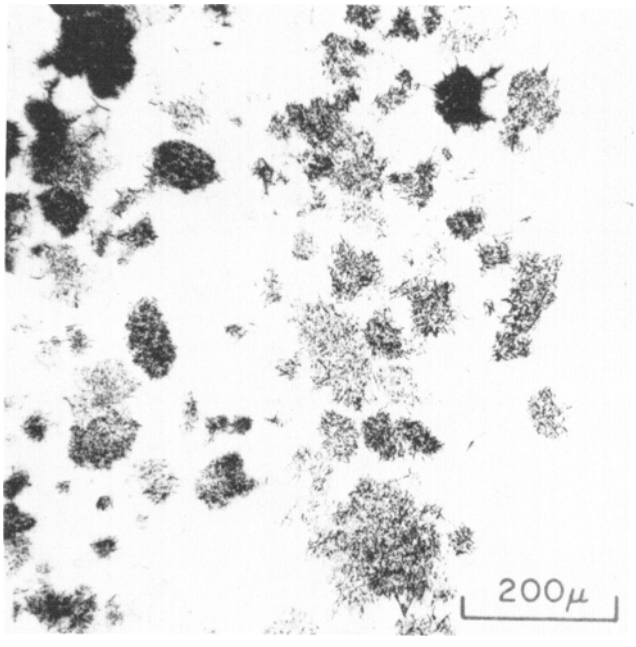

Fig. 9—Optical micrograph showing both types of α after 100 min at 400 °C; the darkly etched regions contain sympathetic α, while the apparently clear unetched areas contain the uniform product.

α precipitates forming randomly in the grain interior (Fig. 10). This reduced number of internal α-precipitates reflects the lower driving force for α nucleation as T_a approaches the β-transus.

Figure 11 is a schematic *T-T-T* diagram which summarizes these various precipitation regimes. It should be emphasized that this particular aging study is based strictly upon small β-ST specimens that have been quenched and isothermally aged. As primary α is introduced into this alloy, or as the β dislocation structure is altered by working, these curves will shift. At present we have not studied dislocation structure effects in a specific way, although by analogy to other β-alloys we would expect high dislocation densitites to accelerate α-phase formation markedly.[14] Our limited work with primary α bearing material indicates that only minor repositioning of these curves takes place as α_p content is altered. Specifically, increasing the α content tends to suppress ω, and thereby increase the tendency for precipitation of coarse plates. The curves are also highly dependent on rate of heating to T_a. For example, β-ST specimens aged in an air furnace at 500 °C for 1 h showed only nondescript uniform precipitation. Presumably this was due to slower specimen heat-up, and an increased time in the uniform α region of Fig. 11. As indicated in this figure, continued aging in the higher temperature regime does not cause the fine uniform α to be replaced by sympathetic plates.

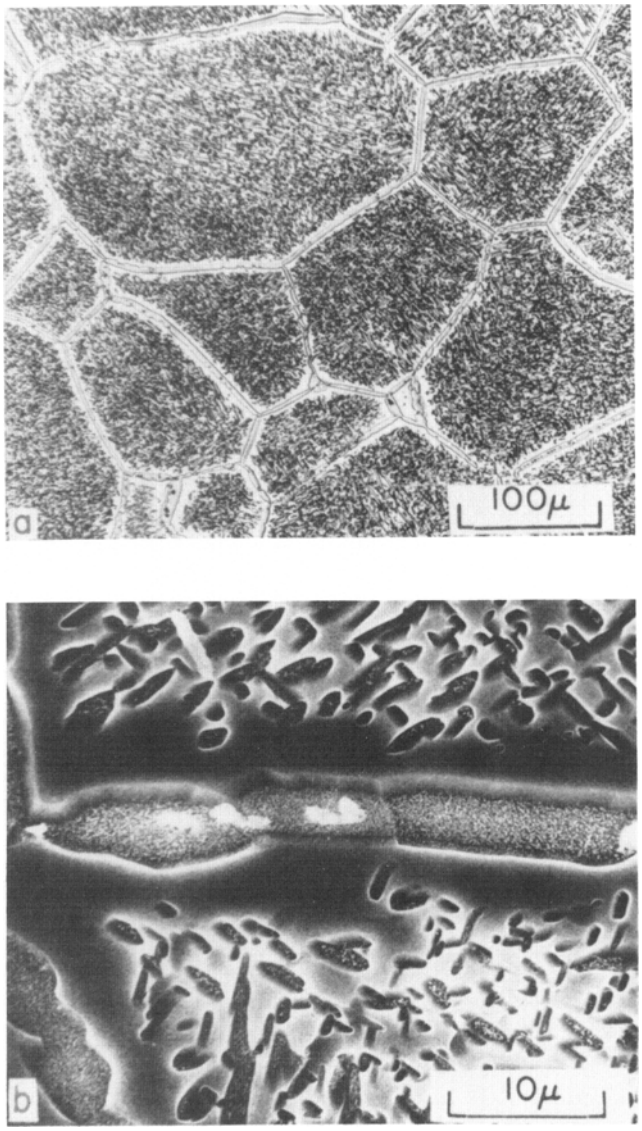

Fig. 10—Grain boundary α layers in β-ST + aged (680 °C—2000 m) Ti-10-2-3: (*a*) optical micrograph, (*b*) SEM micrograph. Note inclusions collected along grain boundary.

D) STRESS ASSISTED TRANSFORMATION

As mentioned earlier, 10-2-3 is sufficiently stabilized to prevent the athermal formation of martensitic products upon quenching. As in other Ti systems, however, the application of a relatively small external stress to the solution treated and quenched structure leads to the formation of martensite. In 10-2-3, X-ray diffraction has shown that the martensitic product has the orthorhombic structure characteristic of α''.[15] This α'' structure has atoms positioned at (0, 0, 0), ($a/2$, $b/2$, 0), (0 $2b/3$, $c/2$,), ($a/2$, $b/6$, $c/2$). Specifically, the lattice parameters are:

$a = 3.01$ Å
$b = 4.83$ Å
$c = 4.62$ Å.

Examples of the stress induced α'' phase are shown in Fig. 12. Note in Fig. 12(*a*) that α'' plates seldom terminate within a grain. Instead, the plates propagate through the β grain until either a grain boundary or another plate is encountered.

A small amount of mechanical twinning of the {112} <111> type has also been observed by TEM in 10-2-3. These plates are optically indistinguishable from α'' and thus no attempt has been made to determine the relative volume fractions of α'' and twinned β.

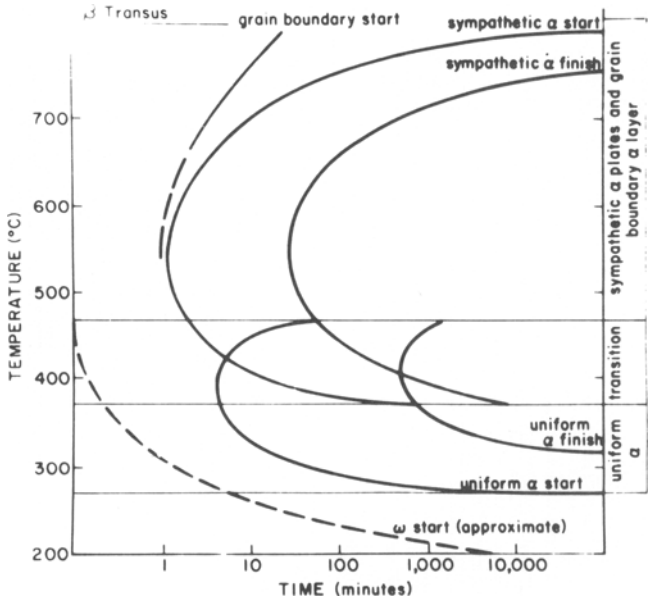

Fig. 11—Qualitative *TTT* diagram for β-ST Ti-10-2-3, illustrating the competition between nucleation regimes.

II. Mechanical Behavior

The effects of the aforementioned microstructural variations on simple stress-strain relations during tensile testing have been briefly examined. Some of the more important results are summarized in Table 1, and are discussed below.

A) SOLUTION ANNEALED CONDITIONS (UNAGED)

Both the β-St and the $\alpha + \beta$-ST conditions of 10-2-3, shown in Fig. 2(*a*) and (*b*), are microstructurally simple. Nevertheless, they possess some very interesting tensile characteristics. When discussing strength levels of various $\beta + \alpha_p$ unaged structures, one should consider the relative importance of three contributions:

1) Second phase strengthening by the α_p dispersion.

2) Solid solution strengthening of the β matrix by solute enrichment.

3) The relation between mechanical stability of the β-phase, and the β composition.

Due to the large α_p spacing and to the large plastic strains associated with α'' formation, only the last of the three is important when discussing the mechanical behavior of ST 10-2-3.

The β-phase is far more unstable in quenched β-ST 10-2-3 than in quenched β + 30 pct α-ST. Consequently β-ST material is far more susceptible to the stress-induced transformation discussed above. Figure 13 compares yield stress, UTS, and elongation to failure for three levels of β stability. Note that while the UTS values are experimentally identical, the yield stresses are drastically different. The stress-strain curves illustrate this effect. In β-ST material, the β-α'' transformation initiates the onset of plastic strain at stresses as low as 250 MPa. The driving force for α'' nucleation is provided by the elastic strain energy of the β matrix. The first plates to nucleate are free to extend the full length of the β grain, and may, in fact, provide nucleation sites in an adjacent grain (Fig. 12). The large increase in martensitic volume fraction per plate and the resulting large plastic strain increment associated with each nucleation event accounts for the apparent "easy glide" region directly following yield. Since the β matrix is being "consumed" by the α'', plates nucleated at a later time transform less β, and thus a smaller plastic strain is associated to each nucleation event. In addition to this, the nucleation frequency must lessen. Thus, an inflection point is observed in the σ-ϵ curves, followed by a rapid rise in σ (ϵ). This rapid rise may also be partly due to second phase strengthening by the α'' plates. The result of this rapid strain hardening is an extended plastic region prior to failure.

The effect of inclusions on the mechanical behavior of 10-2-3 was only qualitatively investigated since no

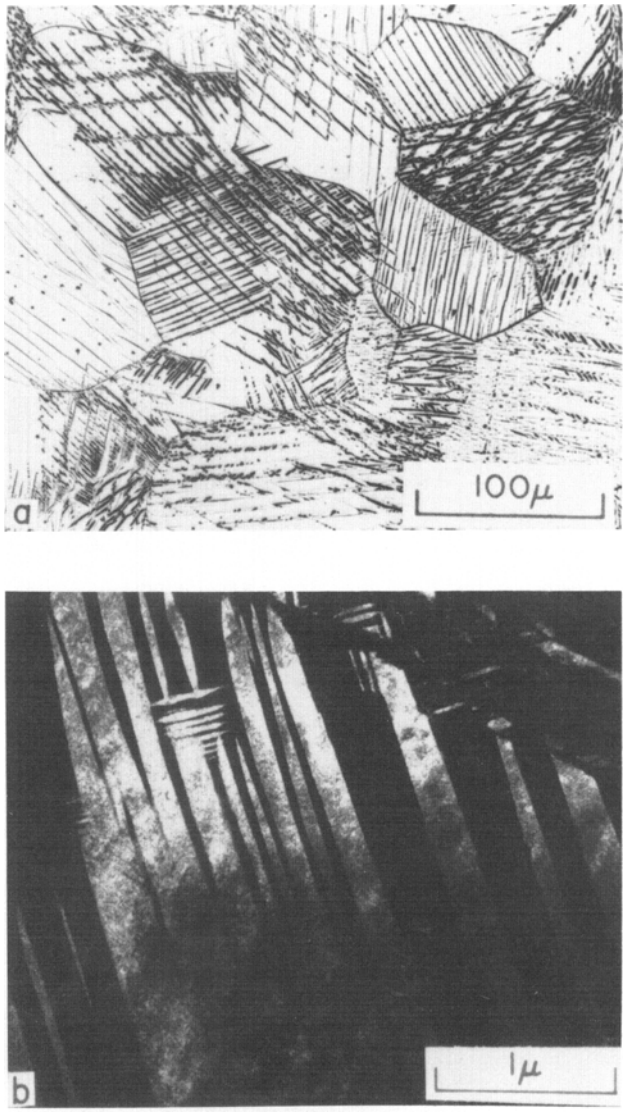

Fig. 12—Microstructures of deformed β-ST material. (*a*) optical micrograph, (*b*) TEM darkfield micrograph.

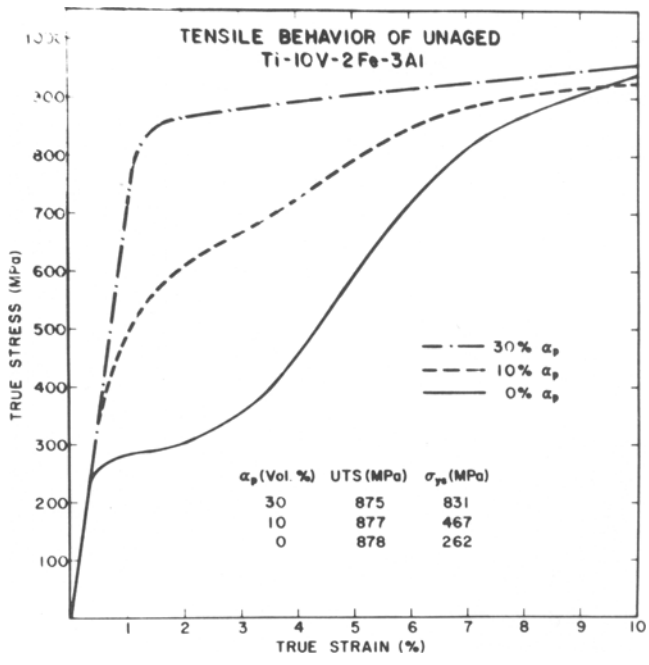

Fig. 13—True stress-strain curves for three levels of β stability.

inclusion free material was available for comparison. Figure 14(*a*) shows the tensile fracture surface of a β-ST specimen. The simple size correlates very well with the inclusion spacing and, in fact, an inclusion can be found in virtually every dimple. Figure 14(*b*) shows the fracture surface of an $\alpha + \beta$ ST-specimen (30 pct α_ρ). Here the one-to-one dimple-inclusion correlation is poorer and instead the dimples appear to correlate more closely to the α_ρ dispersion. From this we conclude that in the absence of coarse α particles, inclusions may act as crack nucleation sites, but that when α_ρ is present, it also plays a role in void nucleation.

The athermal ω found in the ST and quenched conditions does not seem to have any great effect on mechanical response, but since this condition cannot be tested without ω_a, such effects cannot be accurately determined.

B) β-SOLUTION TREATED AND AGED CONDITIONS

Specimens with low volume fractions of ω were characterized by very low work hardening rates and uniform ductilities. Specimens with higher ω volume fractions were brittle, and fractured without macroscopically yielding. Specimens aged for 12 h at 300 °C and tested in compression were also completely brittle and shattered during testing. There have been attempts in the past to understand the brittle nature of β alloys containing the ω-phase.[16-18] We agree that this type of behavior can only result from particle shearing. Shearing acts to destroy the ω particles and results in localized reductions in flow stress and in high dislocation concentrations in narrow slip bands. The resulting pile-ups at grain boundaries may result in stress concentrations, void nucleation, and rapid premature fracture.

All β-ST specimens aged in the uniform α regime of Fig. 11 also were brittle. The strength levels of these fine precipitate dispersions are expected to be very high. The nature of this brittle mechanism is unclear, but work is currently underway to better understand this phenomenon. Transition region specimens are also quite brittle. For example, at 400 °C, specimens aged for 10, 100, and 1000 min all failed prior to yield. It should be noted, however, that all specimens containing fine uniform α are not necessarily brittle, only that aged β-ST specimens containing fine α are brittle β-ST specimens that lie entirely in the plate α regime have reasonable ductilities coupled with high strengths. As shown in Table 1, yield stresses of 1250 MPa with 9 pct elongation to failure are obtainable.

C) $\alpha + \beta$ SOLUTION TREATED AND AGED CONDITIONS

All aging treatments discussed above were preceded by a β-ST. Commercially, it is more useful to study the aging response in $\alpha + \beta$ ST specimens. Although the small amounts of α_ρ present after commercial $\alpha + \beta$ ST do not seem to affect the basic microstructural findings above, there are important effects of α_ρ on the mechanical response of aged 10-2-3.

As we discussed earlier, during $\alpha + \beta$ solution treating, the selection of the ST temperature controls the extent of recrystallization, the volume fraction of α_ρ, and the β matrix composition; and thus the volume fraction of α-phase precipitated during aging. Therefore, as the ST temperature increases, strength also increases. Conversely, ductility can be improved at the expense of strength by decreasing the ST temperature. The brittleness of the above mentioned uniform α regime and the ω regime can then be avoided by reducing the ST temperature. This allows us to produce identical strength levels, in samples strengthened with several different types of second phase precipitation.

Figure 15 shows σ-ϵ curves which demonstrate this point. The first microstructural condition (Condition I) contains ~35 pct globular α_ρ and an unrecrystallized β matrix strengthened with fine nondescript ω. Condition II contains 25 pct α_ρ in an unrecrystallized β + fine α matrix. Condition III has no primary α, is fully

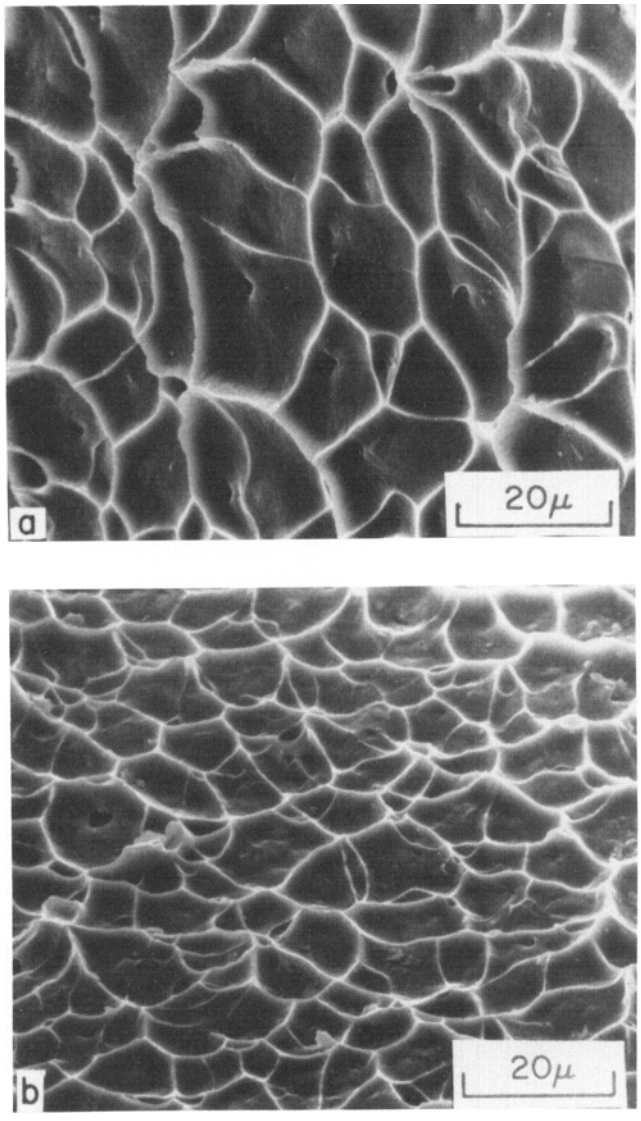

Fig. 14—SEM fractographs of unaged (*a*) β-ST tensile, and (*b*) $\alpha + \beta$-ST (with ~30 pct α_ρ) tensile specimens.

Table I. Selected Tensile Results of ST and Aged Ti-10V-2Fe-3Al

Microstructure	Heat Treatment	Yield Strength, MPa	Ultimate Tensile Strength, MPa	Uniform Elongation, Pct	Elongation to Failure, Pct	Reduction in Area, Pct
20 pct α_p + β + ω_{ath}	730 °C (48 h) + WQ	741	862	9.7	18.6	35
β + ω_{ath}	850 °C (2 h) + WQ	262	878	15.7	21.8	32
α + β + ω_{iso}	700 °C (300 m) + WQ + 250 °C (6000 m)	1218	1266	0.26	0.58	2.25
β + ω_{iso}	850 °C (2 h) + WQ + 250 °C (10^4 m)	Brittle-no yield	—	0	0	0
20 pct α_p + β + α (uniform)	720 °C (100 m) + WQ + 370 °C (1000 m)	1240	1430	2.7	8.9	16
β + α (uniform)	850 °C (100 m) + WQ + 370 °C (1000 m)	Brittle-no yield	—	0	0	0
20 pct α_p + β + α (sympathetic)	730 °C (12 h) + WQ + 500 °C (60 m)	1063	1106	4.6	17.5	58
β + α (sympathetic)	850 °C (100 m) + WQ + 500 °C (240 m)	1225	1243	2.3	8.7	14

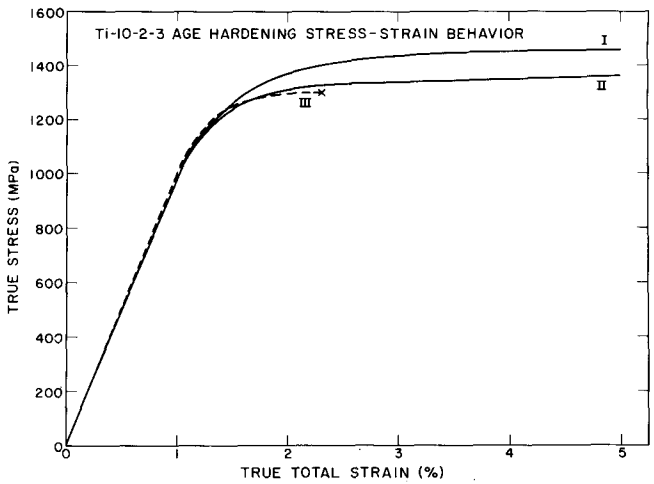

Fig. 15—True stress-True strain curves for three equal strength microstructural conditions of 10-2-3.

recrystallized, and is strengthened by relatively coarse α plates and grain boundary α.

The curve corresponding to the ω bearing specimen, is characterized by a very low work hardening rate, low UTS, and low ductility. Again these characteristics typify systems strengthened by shearable particles. There is evidence that the ductility of these β-ω dispersion can be improved by reducing the sizes of the β-grains and the α_p particles, since this helps to homogenize slip.

Both the β + α conditions demonstrated far better ductilities than the ω condition. The principal differences between the two are their work hardening behaviors and their ultimate tensile strengths. Conditions containing fine α are consistently characterized by higher over-all work hardening, and, as a result, higher UTS values.

SUMMARY

Detailed microstructural work has revealed a number of transformations and transformation products which may occur in Ti-10-2-3.

1) *Athermal omega* appears upon rapid quenching of ST material. Although these fine nondescript particles have no discernible effect on mechanical properties, they affect subsequent aging behavior by catalyzing isothermal ω-phase formations.

2) *Isothermal omega* is discussed as the continued displacive-growth of athermal omega. Three morphologies of omega are shown: nondescript, ellipsoidal, and cuboidal. A rationale for these morphologies is presented. Microstructures containing isothermal omega are generally characterized by low work hardening rates and low ductilities.

3) *Uniform alpha* of both the Burger's and non-Burger's variety was found at low aging temperatures (below 400 °C). This type of α appears to nucleate on particles of isothermal omega. With continued aging this α changes from a blocky morphology into fine "stubby" plates uniformly distributed throughout the β matrix. The fine nature of these dispersions allows very high strengths to be achieved, even in ST specimens containing as much as 25 pct α_p.

4) *Sympathetic plate alpha* of both the Burger's and non-Burger's type was observed above 400 °C. These precipitates were shown as large plates of very high aspect ratio. The sympathetic nature of precipitation

was demonstrated by examining the competition of this mechanism with the uniform mechanism of above. Although these coarser plates do not strengthen as efficiently as the fine uniform dispersions, very high strengths are nonetheless achievable in β-ST material.

5) *Grain boundary alpha* is present above 400 °C, but appears in increasing thickness as the aging temperature is increased. The propensity for α formation at grain boundaries relative to the grain interiors increases as aging temperatures are increased.

6) *Orthorhombic martensite* (α'') is found only in stressed 10-2-3. The transformation can be inhibited by the precipitation of α, and the associated chemical stabilization of β. The formation of α'' decreases yield stresses by plastically accommodating relatively small elastic strains.

In addition to the above transformations, inclusions were found. Analytical STEM techniques showed these inclusions to be rich in Ti, P, S, and Si. Chemical banding, which is found in many other β alloys, was demonstrated to be due to iron segregation.

ACKNOWLEDGMENTS

We gratefully acknowledge the experimental assistance of M. Glatz, G. Biddle, S. Swierzewski, E. Danielson, and N. T. Nuhfer. The X-ray diffraction identification of the α'' phase was done by R. Middleton of AMMRC, Watertown, MA. The drawings were made by R. Miller and the manuscript was typed by Mrs. A. M. Crelli. This work has been supported by the Office of Naval Research under contract N00014-76-C-0409. Facilities for this research are provided by the Center for the Joining of Materials.

REFERENCES

1. T. W. Duerig: Ph.D. Thesis, Carnegie-Mellon University, Pittsburgh, PA, 1980.
2. J. A. Hall: Unpublished research, Timet, Henderson, NV, 1978.
3. C. Chen and R. R. Boyer: *J. Metals,* 1979, vol. 31, p. 33.
4. Y. A. Bagaryatski, T. V. Tagvnova, and G. I. Nosova: *Dokl. Akad, Nauk SSSR,* 1955, vol. 105, p. 1225.
5. D. de Fontaine, N. E. Paton, and J. C. Williams: *Acta Met.*, 1971, vol. 19, p. 1153.
6. H. E. Cook: *Acta Met.*, 1974, vol. 22, p. 239.
7. J. M. Silcock: *Acta Met.*, 1958, vol. 6, p. 481.
8. M. J. Blackburn and J. C. Williams: *Trans. TMS-AIME,* 1968, vol, 242, p. 2461.
9. W. G. Brammer and C. G. Rhodes: *Phil. Mag.,* 1967, vol. 16, p. 477.
10. B. S. Hickman: *J. Matls. Sci.,* 1969, vol. 4, p. 554.
11. J. C. Williams and M. J. Blackburn: *Trans. TMS-AIME,* 1969, vol. 245, p. 2352.
12. C. G. Rhodes and J. C. Williams: *Met. Trans. A.,* 1975, vol. 6A, p. 2103.
13. H. I. Aaronson: *Decomposition of Austenite by Diffusional Processes*, V. F. Zackey and H. I. Aaronson, eds., p. 481, Interscience, New York, 1962.
14. *c.f.* L. A. Rosales and A. W. Sommer: Technical Report NA-73-191, North American Rockwell, Los Angeles, CA.
15. *c.f.* J. C. Williams: *Titanium Science and Technology,* R. Jaffee and H. M. Burte, eds., vol. 3, p. 1433, Plenum Press, New York, 1973.
16. J. C. Williams, B. S. Hickman, and H. L. Marcus: *Met. Trans.*, 1971, vol. 2, p. 1913.
17. A. Gysler, G. Lütjering, and V. Gerold: *Acta Met.*, 1974, vol. 22, p. 901.
18. R. G. Baggerly and J. C. Williams: Unpublished research, Rockwell International Science Center, Thousand Oaks, CA 1974.